Hindawi Publishing Corporation
Advances in Condensed Matter Physics
Volume 2013, Article ID 409620, 11 pages
http://dx.doi.org/10.1155/2013/409620

Research Article

Synthesis, Characterization, and Low Temperature Sintering of Nanostructured $BaWO_4$ for Optical and LTCC Applications

S. Vidya,[1] Sam Solomon,[2] and J. K. Thomas[1]

[1] *Electronic Materials Research Laboratory, Department of Physics, Mar Ivanios College, Thiruvananthapuram, Kerala 695015, India*
[2] *Dielectric Materials Research Laboratory, Department of Physics, St. John's College, Anchal, Kollam District, Kerala 691306, India*

Correspondence should be addressed to J. K. Thomas; jkthomasemrl@yahoo.com

Received 30 May 2013; Accepted 5 August 2013

Academic Editor: Jörg Fink

Synthesis of nano-$BaWO_4$ by a modified combustion technique and its suitability for various applications are reported. The structure and phase purity of the sample analyzed by X-ray diffraction, Fourier transform Raman, and infrared spectroscopy show that the sample is phase pure with tetragonal structure. The particle size from the transmission electron microscopy is 22 nm. The basic optical properties and optical constants of the nano $BaWO_4$ are studied using UV-visible absorption spectroscopy which showed that the material is a wide band gap semiconductor with band gap of 4.1 eV. The sample shows poor transmittance in ultraviolet region while maximum in visible-near infrared regions. The photoluminescence spectra show intense emission in blue region. The sample is sintered at low temperature of 810°C, without any sintering aid. Surface morphology of the sample is analyzed by scanning electron microscopy. The dielectric constant and loss factor measured at 5 MHz are 9 and 1.56×10^{-3}. The temperature coefficient of dielectric constant is −22 ppm/°C. The experimental results obtained in the present work claim the potential use of nano $BaWO_4$ as UV filters, transparent films for window layers on solar cells, antireflection coatings, scintillators, detectors, and for LTCC applications.

1. Introduction

The ever increasing scientific and technological demand for novel materials with unique properties poses challenges to scientific research. Nanomaterials have caught the interest of researchers because of its exceptional properties which are completely different from its bulk material. Synthesis of advanced functional materials in nanoscale is one of the prime fields of interest.

Generally, AWO_4 (A = Ba, Sr, Ca, Pb) tetragonal scheelite-type crystals of divalent metal ion tungstate have been of immense interest because of their remarkable properties such as luminescence, nonlinear optical activity, photocatalysis, and scintillation [1–7]. Among them, $BaWO_4$ is a significant material due to its excellent PL emission and stimulated Raman scattering active crystal. The reasons for blue and green PL emissions of $BaWO_4$ are discussed in many different aspects ranging from defect centers by interstitial oxygen atoms to structural disorder in the crystal lattice [8–11]. $BaWO_4$ also serves as a potential material for designing all solid-state lasers, especially that it has been considered as a unique Raman crystal for a wide variety of pump pulse durations in Raman laser pulses [12–17]. Its other applications include nuclear spin optical hole burning hosts [6], radiation detection [1], scintillating devices [4], and other electro-optic applications [1]. Since the properties of materials can be tuned by its microstructure, different morphological $BaWO_4$ such as nanowires, spheres, cylinders, whiskers, penniform $BaWO_4$ nanostructures, and flower-like structures were prepared [18–23] and methods like solid-state reaction [24–26], hydrothermal-method [9, 27–29], Czochralski [30–33], high temperature flux crystallization [34], polymeric precursor chemical route [35], microwave-assisted synthesis [36, 37], and micro emulsions-based routes [19, 38] were employed for the synthesis.

However, even though the luminescent behavior of scheelite $BaWO_4$ remains much investigated, its other optical constants and dielectric applications are not much explored. Hence, in the present work we have specifically concentrated on the studies of the suitability of nano-$BaWO_4$ powders,

synthesized through a single step modified combustion technique, for their various optical as well as electrical applications. In addition, we report the results of structural characterization, photo luminescence, sintering behavior, and dielectric performance. Prime novelty of our study is the sintering of nano-$BaWO_4$ at a very low temperature of 810°C for the first time without any sintering aid, which points out its use as a low temperature cofired ceramic (LTCC). We have also investigated detailed optical studies of the compound owing to its tremendous potential for application as UV filters, sensors, and transparent conducting oxide films for solar windows.

2. Experimental

Even though there are various methods reported for the synthesis of $BaWO_4$, many of them need high processing temperatures, long reaction time, postcalcinations, and sophisticated equipments as well. In the following years, the scientific community is in search of the development of easy, economical, and nonhazardous preparation techniques with which we can control the size and shape of the particles in order to tune their properties. In this context, a widely used combustion technique is very relevant that it is cost effective and time saving and provides high quality phase pure nanoproduct [39].

For the preparation of nano-$BaWO_4$, we opted a modified combustion process using ammonia and citric acid which were used as fuel and complexing agent, respectively. Aqueous solutions containing Ba and W ions were prepared by dissolving stoichiometric amounts of $Ba(NO_3)_2$ and ammonium paratungstate in double distilled water. Citric acid was then added to the solution as complexing agent. Oxidant to fuel ratio of the system was adjusted by adding concentrated nitric acid and ammonium hydroxide solution and the ratio was kept at unity. The precursor solution of pH ~7.0 was then heated using a hot plate at ~250°C in a ventilated fume hood. The solution boils on heating, and undergoes dehydration accompanied by foam. On persistent heating the foam gets autoignited giving a voluminous fluffy nanopowder of $BaWO_4$.

Structure of the as-prepared powder was examined by powder X-ray diffraction (XRD) technique using a Bruker D-8 X-ray diffractometer with nickel filtered Cu K_α radiation. Particulate properties of the combustion product were examined using transmission electron microscopy (TEM, Model-Hitachi H-600 Japan) operating at 200 kV. The Infrared (IR) spectra of the samples were recorded in the range 400–4000 cm^{-1} on a Thermo-Nicolet Avatar 370 Fourier transform infrared (FT-IR) spectrometer using KBr pellet method. The Fourier transform-Raman spectrum of the nanocrystalline $BaWO_4$ was carried out at room temperature in the wave number range 50–1200 cm^{-1} using Bruker RFS/100S Spectrometer at a power level of 150 mW and at a resolution of 4 cm^{-1}. The samples were excited with an Nd:YAG laser lasing at 1064 nm, and the scattered radiations were detected using Ge detector. The photoluminescence (PL) spectra of the samples were measured using FluoroLog-3 Spectrofluorometer. The photons from the source were filtered by an excitation spectrometer. The monochromatic radiation was then allowed to fall on the disc samples, and the resulting radiation was filtered by an emission spectrometer and then fed to a photomultiplier detector. The variation of intensity was recorded as a function of wavelength. The optical measurements of the nanopowder were carried out at room temperature using a Cary 100 BIO UV-VIS spectrophotometer in the wavelength range from 200–700 nm. The sample for the analysis was a 2 mM solution of $BaWO_4$ prepared by dispersing the nanopowder in ethanol taken in 1 : 20 volume ratio. The same solvent was used as the blank for the analysis in order to calibrate the spectrophotometer.

To study the sinterability of the nanoparticles obtained by the present combustion method, the as-prepared $BaWO_4$ nanoparticles were mixed with 5% polyvinyl alcohol and pressed in the form of cylindrical pellet of 12 mm diameter and ~2 mm thickness at a pressure about 350 MPa using a hydraulic press. The sintering temperature pellet was optimized at 810°C for 3 h after conducting many trials. The surface morphology of the sintered sample was examined using scanning electron microscopy (SEM, Model-JEOL JSM 5610 LV). For low frequency dielectric studies, the pellets were made in the form of a disc capacitor with the specimen as the dielectric medium. Both the flat surfaces of the sintered pellet were polished and then electroded by applying silver paste. The capacitance of the sample was measured using an LCR meter (Hioki-3532-50 LCR HiTester) in the frequency range 100 Hz–5 MHz at different temperatures from 30 to 250°C.

3. Results and Discussion

The XRD pattern of the as-prepared $BaWO_4$ nanopowder is shown in Figure 1. All the peaks including the minor ones are indexed for a perfect tetragonal scheelite with space group $I4_1/a$. This clearly shows that the $BaWO_4$ phase formation was complete during the combustion process itself without the need for any postcalcinations step. In the case of solid state synthesis of $BaWO_4$ [23], the mixture is ball milled for 24 h and calcined at 800°C in order to obtain the required phase. Thus, modified combustion method offers an economic and time saving technique since the as-prepared powder itself is phase pure without any calcination at high temperature.

The lattice constants calculated from the XRD are $a = b = 5.5609$ and $c = 12.7123$ Å. The calculated values of lattice constants are consistent with that reported in JCPDS NO 72-0746. The small variations in the values could be due to the quantum size effect of nanoparticles and the rapid formation kinetic energy of $BaWO_4$ during the combustion process, resulting in a small distortion of the lattice. The crystallite size calculated from full width at half maximum (FWHM) using Scherrer formula is ~20 nm.

Figure 2 shows the TEM image and selected area electron diffraction (SAED) pattern of as-prepared nano-$BaWO_4$ nanoparticles. The average particle size calculated from the TEM micrograph is 22 nm. The particles in the TEM image are not agglomerated which points to the excellent crystalline nature of the nanopowder. SAED pattern have a number of bright polycrystalline concentric diffraction rings. The rings are diffused and hollow showing that the products are composed of nanocrystals with different orientations.

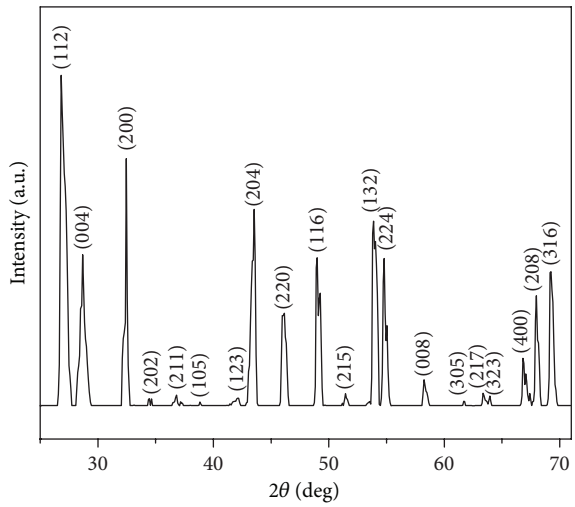

Figure 1: XRD pattern of as-prepared $BaWO_4$ nanopowder.

The electrons reflected and diffracted from the different crystallographic planes of the unit cells of $BaWO_4$ produce these bright spots. These well distinguished rings are a clear evidence of the high crystalline nature of the sample.

Vibrational spectroscopy is a fine method for investigating the structural details of a compound. In order to understand the degree of structural disorder of the scheelite $BaWO_4$ nanopowder, FT-Raman and FT-IR spectra of the sample are recorded and are given in Figures 3 and 4, respectively.

In tetragonal scheelite phase, Ba atoms are surrounded by eight oxygen atoms, and tungsten atoms are surrounded by four oxygen atoms in tetrahedral configuration to form $[WO_4]^{2-}$. It is reported by Basiev et al. [40] that the primitive cell of the tungstate crystal includes two formula units, and the Raman spectra of scheelite crystals can be divided into two groups, internal and external. The first is called lattice phonon mode which corresponds to the motion of Ba^{2+} cation and the rigid molecular unit. The second belongs to the vibration of inside $[WO_4]^{2-}$ molecular units with the centers of mass stationary.

Raman-active phonon modes can be employed to estimate the structural order at a short range of a material. The group theory calculation presents 26 different vibrations for the $BaWO_4$, which is represented by [40, 41]

$$\Gamma = 3A_g + 5A_u + 5B_g + 3B_u + 5E_g + 5E_u, \quad (1)$$

where all A_g, B_g, and E_g modes are Raman-active in which E_g modes are doubly degenerate, A_g and B_g modes are nondegenerate and the odd modes $4A_u$ and $4E_u$ can be registered only in FT-IR spectra. The three B_u modes are silent ones, whereas one A_u and E_u modes are acoustic vibrations. Thus, we expect 13 Raman-active modes in $BaWO_4$.

All the observed Raman modes are the characteristics of a scheelite tetragonal [9, 40–42]. The internal modes $\nu_1(A_g)$, $\nu_2(E_g)$, $\nu_3(E_g)$, and $\nu_4(B_g)$ were observed at 924, 842, 790, 361, 345, and 326 cm^{-1}. The free rotation mode was detected at 190 cm^{-1}, and the external modes were localized at range 141–78 cm^{-1}.

The FT-IR spectra of the $BaWO_4$ were carried out in transmittance mode. Since $BaWO_4$ has tetrahedral symmetry (T_d), only $F_2(\nu_3, \nu_4)$ modes are infrared active. A strong absorption peak at 410 cm^{-1} can be assigned to $F_2(\nu_4)$ vibration mode which represents the bending vibration of W–O. The antisymmetric stretching vibration $F_2(\nu_3)$ originating from the W–O in WO_4^{2-} tetrahedron corresponds to the broad intense peak at 823 cm^{-1}. Besides this strong band, a medium intense band can be seen in the region 632 cm^{-1} which can be attributed to W–O antisymmetric stretching vibrations. Our results match well with the early reported literatures [37, 42].

The absence of two B_g modes and small discrepancy observed in the Raman-active modes when compared to early reports [37–40] may be due to the different preparation method, average crystal size, and structural disorder degree in the lattice. The absence of certain modes and activeness of modes at same regions of IR and Raman spectra points to the lowering of symmetry of crystal structure leading to short range distortion of crystal lattice which exactly corroborates with the XRD results.

The UV-Visible absorption, reflectance, and transmission spectra of nano-$BaWO_4$ are shown in the Figures 5(a), 5(b), and 5(c), respectively. Sample shows maximum absorption in the UV region with a steep absorption edge centered at 254 nm. At the visible region, the sample is nearly 63% transparent while its reflectance is almost 18%. Maximum absorption in the UV region along with uniform transparency in the visible region makes the sample ideal for UV sensors, filters, and screening applications. Also, the property of high transmittance and low reflectance in the visible region makes the material a good candidate for transparent windows in solar cells.

The Wood and Tauc [43] equation was used to estimate the optical band gap of nano-$BaWO_4$ nanopowder. According to this equation, the optical band gap energy is related with absorbance and photon energy by the following equation:

$$\alpha h\vartheta = \left(\beta h\vartheta - E_g\right)^m, \quad (2)$$

where β is an energy independent constant, α is the optical absorption coefficient, h is the Planck constant, ν is the frequency of incident photon, E_g is the optical band gap, and m is a constant which characterizes the nature of band transition. $m = 1/2$ and $3/2$ corresponds to direct allowed and direct forbidden transitions, and $m = 2$ and 3 corresponds to indirect allowed and indirect forbidden transitions, respectively. The optical band gap can be obtained from the extrapolation of the straight-line portion of the $(\alpha h\nu)^{1/m}$ versus $h\nu$ plot to $h\nu = 0$.

The optical absorption coefficient α is determined using the relation

$$\alpha = -\ln \frac{T}{d}, \quad (3)$$

where T is the optical transmittance and d is the optical path length through the cuvette.

The variation of α with photon energy is established in Figure 6. The absorption coefficient shows a maximum in

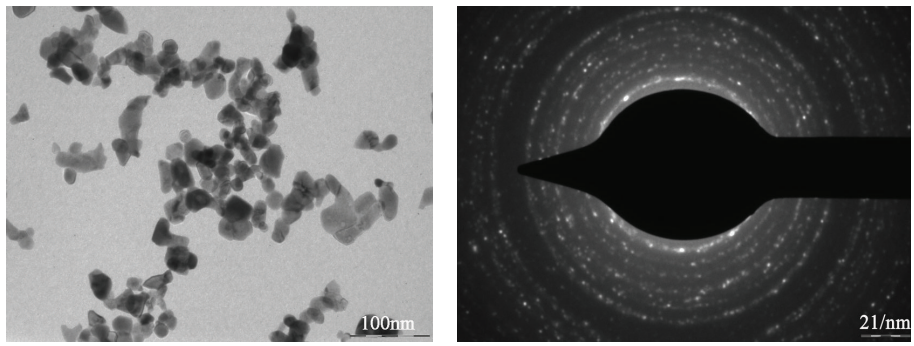

Figure 2: TEM micrograph and SAED pattern of nano-$BaWO_4$.

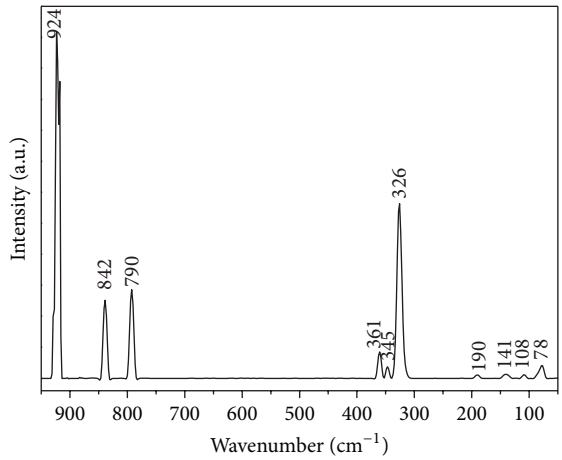

Figure 3: Raman spectrum of as-prepared nano-$BaWO_4$ prepared by combustion technique.

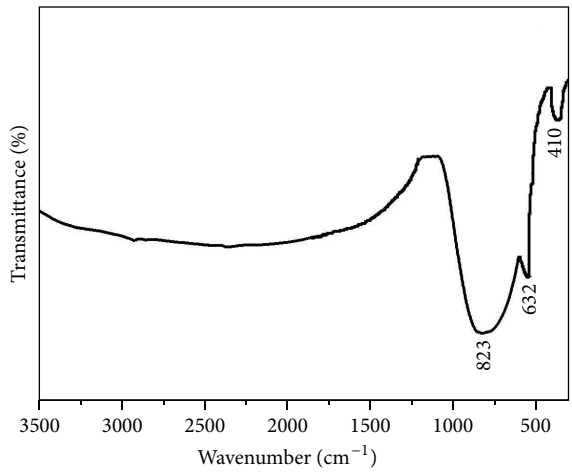

Figure 4: FT-IR spectrum of as-prepared nano-$BaWO_4$ prepared by combustion technique.

the UV region and falls off to NIR region. It shows a maximum at 4.5 eV around 1.23 cm^{-1}. The existence of sharp absorption band is an indication of excellent crystalline nature of the nanosample. The calculated optical band gap is also illustrated in Figure 6. The band gap of the sample is found to be 4.1 ev, which is exactly matching with the value reported by Cavalcante et al. [9], Anicete-Santos et al. [42], and Tyagi et al. [44] for $BaWO_4$. The present obtained value is lower than that reported by Lima et al. [11] which is 5.67 eV. The lowering of band gap can be due to several factors such as changes in local atomic structure, lowering of symmetry of lattice, electro negativity of transition metal ions, connectivity of the polyhedrons, deviation in the O–X–O bonds, oxygen vacancies, distortion of the $[XO_4]^{2-}$ tetrahedrons, and intrinsic surface states [45–47]. From the Raman spectra, it is confirmed that the sample possess certain degree of structural disorder which would have resulted in the formation of intermediate energy levels between the valance and conduction band. As the band gap is the energy difference between valance and conduction band, the presence of these intermediate levels resulted in the reduction of optical band gap energy. AS $BaWO_4$ prepared by the present method possess wide band gap along with good transmittance in the visible region is suitable for transparent conducting oxide films for window layers on solar cells.

The complex refractive index ($n = n + ik$) and dielectric function ($\varepsilon = \varepsilon_1 + i\varepsilon_2$) also characterize the optical properties of any solid material. The normal incidence reflectivity R can be given by [48]

$$R = \frac{(n-1)^2 + k^2}{(n+1)^2 + k^2}, \tag{4}$$

where k is extinction coefficient and n is the refractive index of the sample. The extinction coefficient k indicates the amount of absorption loss when the electromagnetic wave was propagated through the material and can be calculated using the relation [49]

$$k = \frac{\alpha\lambda}{4\pi}. \tag{5}$$

The variation of n and k with photon energy observed for the samples is demonstrated in Figure 7. The refractive index n and extinction coefficient k increase with increasing frequency. The variation of n and k values shows that some interactions took place between photons and electrons in the frequency range studied. It is found that the maximum values

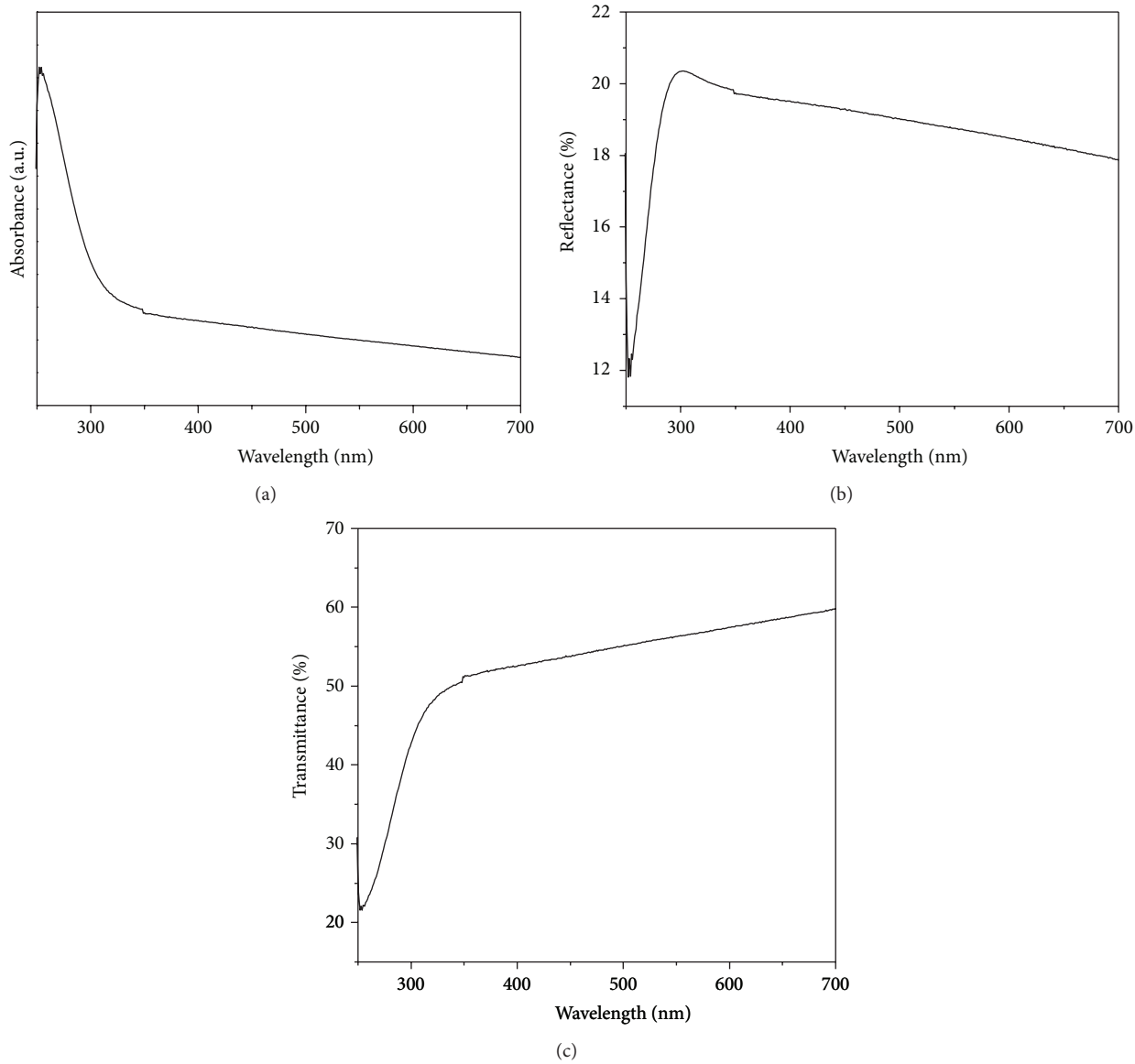

Figure 5: (a) Absorbance, (b) reflectance, and (c) transmittance spectra of nano-$BaWO_4$.

of n and k from the graph are at 2.8 and 3.2×10^{-6}, respectively, which occur at the same photon energy 4.75 eV. The peak values of n and k observed in the UV region indicate that the material can be considered as a good inorganic UV absorber. As $BaWO_4$ has a high refractive index ($n > 1.8$), it causes a large proportion of photons to be trapped by total internal reflections which is the reason for its use as scintillators and as detectors in CRESST for dark matter research [50].

The fundamental electron excitation spectrum of the nanopowder has been described by means of frequency dependence of the complex electronic dielectric constant. The complex dielectric constant is an intrinsic and fundamental property of a material. The real part of the term is associated with how much it will slow down the speed of light in the material, and the imaginary part of the term shows how the dielectric absorbs energy from the electric field due to dipole motion. The real and imaginary parts of the dielectric constant were determined using the relation [51]

$$\varepsilon = \varepsilon_1 + i\varepsilon_2 = (n + ik), \tag{6}$$

where ε_1 and ε_2 are the real and imaginary parts of the dielectric constant, respectively, and are given by

$$\varepsilon_1 = \left(n^2 - k^2\right), \qquad \varepsilon_2 = 2nk. \tag{7}$$

The dependence of ε_1 and ε_2 on photon energy is illustrated in Figure 8. Both ε_1 and ε_2 increase with photon energy and show maximum peaks around 9.25 and 1.28×10^{-5}, respectively, at 4.5 eV.

A material is optically conductive when it shows conductivity on exposure to electromagnetic radiation. The optical

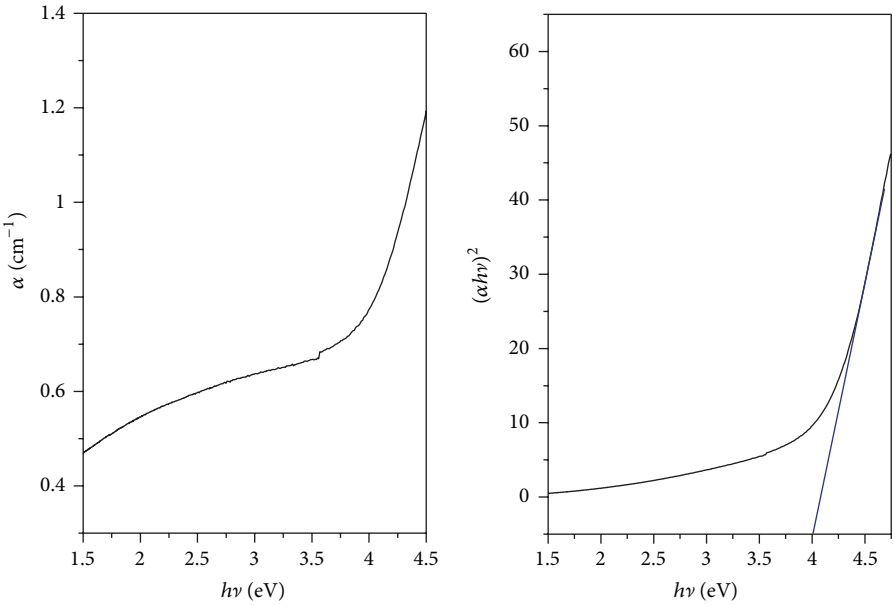

Figure 6: (a) Variation of alpha with photon energy and (b) Tauc's plot of nano-$BaWO_4$.

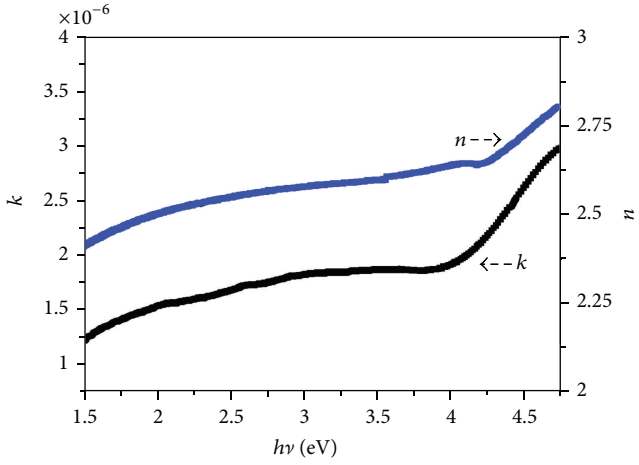

Figure 7: Variation of n and k with photon energy.

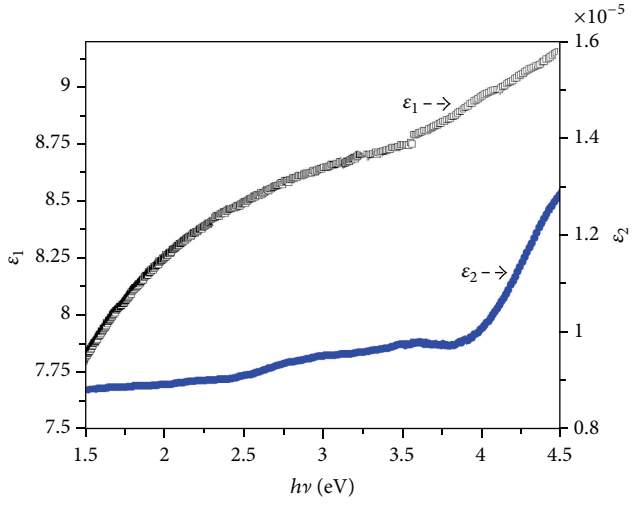

Figure 8: Variation of complex dielectric constants ε_1 and ε_2 with photon energy.

conductivity of the sample is determined using the relation [52]

$$\sigma = \frac{\alpha n c}{4\pi}, \tag{8}$$

where c is the velocity of light.

Figure 9 demonstrates the variation of optical conductivity with incident photon energy. It is seen from the figure that the optical conductivity increases with increasing energy. The reason for the increase in optical conductivity is due to the fact that the electrons are excited by photon energy and possess more kinectic energy than that in its ground state. Optical conductivity shows a value of 6.9×10^9 Sm^{-1} at 4.5 eV and a minimum value of 2.72×10^9 Sm^{-1} at 1.5 eV. The high value of optical conductivity in the visible region indicates that nano-$BaWO_4$ could be ideal for the fabrication of solar cell panels.

The scheelite tungstate compounds are well known for their luminescence activity. The PL emission spectra of as-prepared $BaWO_4$ nanopowder is shown in Figure 10(a). The sample exhibited a broad blue emission peak as expected and a medium intense peak in the green region of the visible spectra. There are several reports which explain the mechanisms responsible by the PL emission in scheelite tungstates. The luminescent properties of $BaWO_4$ are mainly determined by two reasons; the first one is the charge-transfer transitions between the O2p orbits and the empty d orbits of the central W^{6+} ions in $[WO_4]^{2-}$ tetrahedron, [53] and

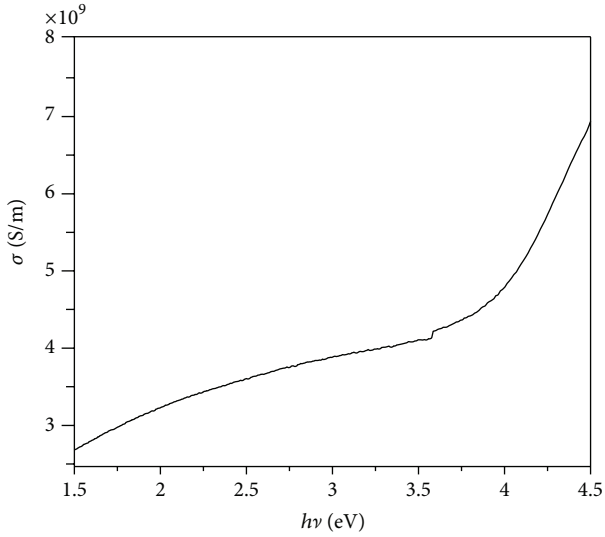

Figure 9: Variation of optical conductivity σ with photon energy.

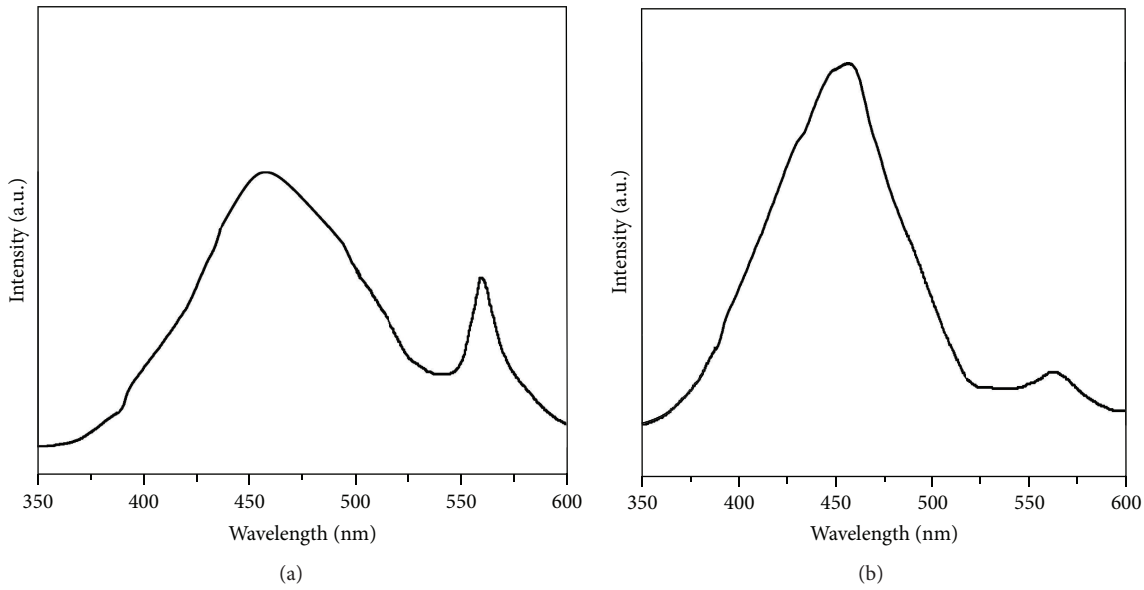

Figure 10: PL spectra of (a) as-prepared and (b) 700°C heated nano-$BaWO_4$.

the second one is due to the structural distortions in the crystal lattice. The tungsten cation ideally tends to bond with four oxygen ions (WO_4), and the barium cation tends ideally to bond with eight oxygen ions (BaO_8 pseudocubic configuration). In the structure, just before the complete ordering at short range, there exist various coordination environments for the W such as WO_3 and WO_4. The existence of WO_3 and distorted WO_4 clusters in the lattice are able to induce the formation of intermediary energy levels within band gap. These energy levels are composed of oxygen 2p states (near the valence band) and tungsten 5d states (below the conduction band). In this case, the polarization induced by the symmetry break and the existence of these localized energy levels are favorable conditions for the formation of trapped holes and trapped electrons. It is generally accepted that the higher energy blue emission of tungstates with scheelite structure is due to the radiative decay of self-trapped excitons localized at the regular $[WO_4]^{2-}$ complexes, and the low energy green emission is associated with structural defects [9–11, 42, 44, 47]. The presence of defective state levels was also confirmed from the UV-Vis analyses.

In order to reduce the structural disorder, the sample was annealed at 700°C for 1 hour, and again the PL spectrum was recorded as the fact that highly disordered and highly ordered structures at short range are not favorable to intense PL emission [42]. The emission spectrum of annealed sample is as in Figure 10(b). Annealing had resulted in an increased intensity of the emission. The blue emission gets intensified while the green emission decreases considerably. The main reason for the diminishing of emission in green region may

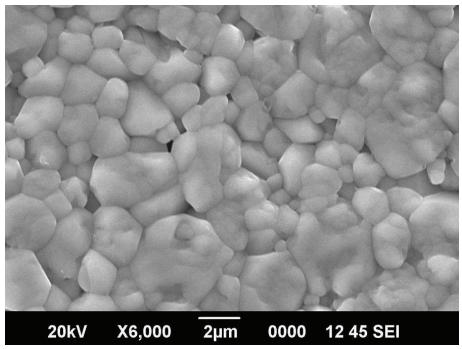

Figure 11: SEM image of sintered $BaWO_4$ pellet.

be due to the fact that high ordering is achieved by the WO_4 and BaO_8 molecular groups due to annealing.

The sintering behavior of the nanocrystals of $BaWO_4$ powder synthesized through the present combustion route was studied. The relative green density of the specimen used for the sintering study was 55%. A sintered density of ~ 95% of the theoretical value was obtained upon sintering the compacted specimen at 810°C for 3 h. It may be noted that the $BaWO_4$ powder prepared through solid state method by earlier Yoon et al. [23] obtained a well sintered pellet at higher temperature of 1150°C. In the present work, the sintering temperature is nearly 340°C lesser than the early reports, and this optimum sintering temperature is achieved without adding any sintering agents. The reduction of sintering temperatures for the nanomaterials when compared to its conventional micro ceramics is mainly due to its higher surface area than the bulk materials. Since sintering start at the surface, availability of large surface area amount to lowering the corresponding temperatures. Thus, we could sinter $BaWO_4$ at a lower temperature of 810°C without any sintering aid, for the first time.

The SEM image of the sintered sample is shown in Figure 11. The surface morphology of sintered sample shows maximum densification. It is observed from the micrograph that the size of the grains has increased from 500 nm to about 2 μm due to sintering, with no cracks and very little porosity.

The dielectric constant ε_r and the loss factor tan δ values of the sintered pellets were studied in the frequency range 100 Hz to 5 MHz at room temperature with silver electrodes on both sides of the circular disc and are given in Figure 12(a). It can be clearly noted that the loss factor decreases as frequency increases, while the dielectric constant remains almost unaltered in high frequency region. The dielectric constant ε_r and loss factor tan δ values of the $BaWO_4$ pellets at 5 MHz in room temperature were ~9 and 1.56×10^{-3}, respectively. The value of dielectric constant is well agreeing with that reported in the literature [23, 54].

The variation of ε_r and tan δ at different temperature ranging from 30–250°C is shown in Figure 12(b). It is clear from the graph that the temperature dependence of dielectric constant is very minimal in the measured temperature range. The loss factor further lowers with increase of temperature and is of order 10^{-3} at temperature above 100°C. At 250°C, the value of ε_r is 8.5 and that of tan δ is 4.5×10^{-4}.

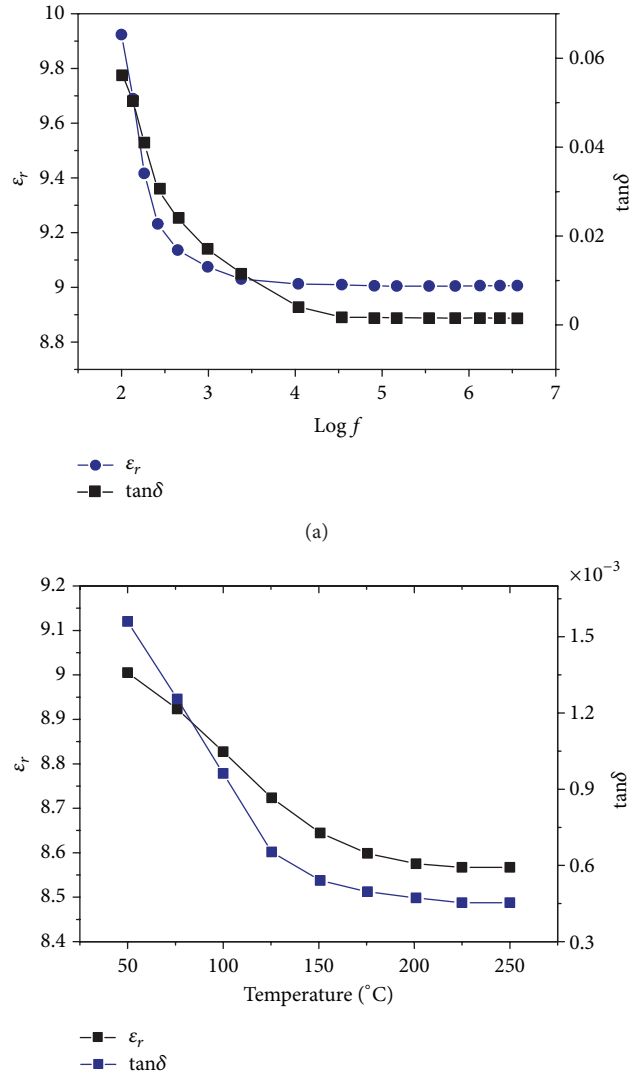

Figure 12: (a) Variation of dielectric constant ε_r and loss factor tan δ with respect to frequencies and (b) with respect to temperature.

The temperature coefficient of dielectric constant (T_{CK}) is determined using the equation given below between temperatures 250°C and 30°C at 5 MHz,

$$T_{CK} = \frac{K_{250} - K_{30}}{220} * \frac{1}{K_{30}} * 10^6, \quad (9)$$

where K_{30} and K_{250} are the dielectric constants at 30°C and 250°C, respectively, and 220 is the temperature difference. The obtained T_{CK} is −22 ppm/°C. Thus, nano-$BaWO_4$ possess negative temperature coefficient of dielectric constant.

The significance of the present work is the development of nanostructured scheelite tetragonal $BaWO_4$, a potential wide band gap semiconductor and transparent conduction oxide material, for optical applications through a modified combustion method. The powder was sintered at a very low temperature of 810°C without any sintering aid for the first time to examine its application as LTCC material.

The accomplishment of this type sintering is that we could get the well densified sample without compromising its properties. Already a few studies on the low temperature sintering of scheelite ceramics using various sintering aid, its dielectric properties, and their suitability as LTCC materials were reported [54–58]. Zhuang et al. [55–57] sintered $Ba_5Nb_4O_{15}$-$BaWO_4$ and $Ba_3(VO_4)_2$-$BaWO_4$ composites at a low temperature of ~900°C and studied its dielectric properties for LTCC application, while the effect of $BaWO_4$ ceramic filler content on the dielectric properties of the $BaWO_4$-poly-tetrafluoroethylene laminates composites for microwave substrate application was investigated by James et al. [58]. Usually, glass and polymer composite materials are used for LTCC applications. But their high values of dielectric loss, thermal mismatch, and high sintering temperature impose restrictions on their effective use as LTCC materials. The doping of sintering aid would result in poor dielectric response such as high loss and low quality factor. $BaWO_4$, in this case, possess a very low tan δ value and low temperature coefficient of dielectric constant. The novelty of our technique is that we could get a glass free as well as dopant free pure ceramic nano material for LTCC applications. The low sintering temperature, dielectric constant, and loss factor make nano structured $BaWO_4$ prepared by the combustion method confirm its suitability as a promising candidate for its application as LTCC, substrate, and electronic packing materials. The negative temperature coefficient values of this compound also ensure the stability of the dielectric permittivity with temperature when it is used as LTCC material in multilayer circuits.

4. Conclusions

Nanocrystalline semiconducting $BaWO_4$ was synthesized through a modified combustion process. The X-ray diffraction studies showed that the nanopowder was single phased with tetragonal structure. The FT-IR and Raman spectral analysis confirm that the as-prepared powder itself is phase pure with a short range distortion. TEM analysis confirms that the nanocrystalline nature of the sample has a mean size of 22 nm. The UV-VIS spectra analysis revealed that the material is a wide band semiconductor of band gap 4.1 eV along with good transmittance in the visible region which makes it suitable for transparent conducting oxide films for window layers on solar cells, warming coatings, solar control, and antireflection coatings. Because of the high refractive index of 2.5, it could be used as scintillators and as detectors in CRESST for dark matter research. The high value of optical conductivity in the visible region indicates that nano-$BaWO_4$ could be ideal for the fabrication of solar cell panels. The nanocyrstalline $BaWO_4$ is found to be a photoluminescent material with emissions in blue and green regions. On annealing green emission intensity decreases which is attributed to the perfect ordering of the crystal. These nanocrystals could be sintered at a relatively low temperature of 810°C to a high density without any sintering aid. The SEM image of the sintered sample indicates that the material achieved high densification. The room temperature dielectric constant (ε_r) and the loss factor tan δ of the sintered pellet at 5 MHz were ~9 and 1.56×10^{-3}, respectively. The temperature coefficient of dielectric constant is −22 ppm/°C. The decrease in sintering temperature, low dielectric constant, and low loss factor indicates that nano-$BaWO_4$ are excellent low temperature cofired ceramics, substrate material, and electronic packing materials.

Conflict of Interests

The authors declare that they have no conflict of interests.

Acknowledgment

The authors acknowledge the Council of Scientific and Industrial Research (CSIR), New Delhi Council, for the financial assistance.

References

[1] M. Nikl, P. Bohacek, E. Mihokova et al., "Excitonic emission of scheelite tungstates AWO_4 (A = Pb, Ca, Ba, Sr)," *Journal of Luminescence*, vol. 87, pp. 1136–1139, 2000.

[2] A. J. Lee, H. M. Pask, J. A. Piper, H. Zhang, and J. Wang, "An intracavity, frequency-doubled $BaWO_4$ Raman laser generating multi-watt continuous-wave, yellow emission," *Optics Express*, vol. 18, no. 6, pp. 5984–5992, 2010.

[3] P. Cerný, H. Jelínková, P. G. Zverev, and T. T. Basiev, "Solid state lasers with Raman frequency conversion," *Progress in Quantum Electronics*, vol. 28, no. 2, pp. 113–143, 2004.

[4] T. T. Basiev, V. Osiko, A. M. Prokhorov, and E. M. Dianov, "Crystalline and fiber raman lasers," in *Solid-State Mid-Infrared Laser Sources*, vol. 89, pp. 359–408, 2003.

[5] J. Ninkovica, G. Angloher, C. Bucci et al., "$CaWO_4$ crystals as scintillators for cryogenic dark matter search," *Nuclear Instruments and Methods in Physics Research A*, vol. 537, no. 1-2, pp. 339–343, 2005.

[6] A. Caprez, P. Meyer, P. Mikhail, and J. Hulliger, "New host-lattices for hyperfine optical hole burning: materials of low nuclear spin moment," *Materials Research Bulletin*, vol. 32, no. 8, pp. 1045–1054, 1997.

[7] P. Afanasiev, "Molten salt synthesis of barium molybdate and tungstate microcrystals," *Materials Letters*, vol. 61, no. 23-24, pp. 4622–4626, 2007.

[8] T. T. Basiev, Y. K. Danileiko, M. E. Doroshenko et al., "High-energy $BaWO_4$ Raman laser pumped by a self-phase-conjugate Nd:GGG laser," *Laser Physics*, vol. 14, no. 7, pp. 917–921, 2004.

[9] L. S. Cavalcante, J. C. Sczancoski, J. W. M. Espinosa, J. A. Varela, P. S. Pizani, and E. Longo, "Photoluminescent behavior of $BaWO_4$ powders processed in microwave-hydrothermal," *Journal of Alloys and Compounds*, vol. 474, no. 1-2, pp. 195–200, 2009.

[10] Y. Yin, Z. Gan, Y. Sun et al., "Controlled synthesis and photoluminescence properties of BaXO4 (X = W, Mo) hierarchical nanostructures via a facile solution route," *Materials Letters*, vol. 64, no. 6, pp. 789–792, 2010.

[11] R. C. Lima, M. Anicete-Santos, E. Orhan et al., "Photoluminescent property of mechanically milled $BaWO_4$ powder," *Journal of Luminescence*, vol. 126, no. 2, pp. 741–746, 2007.

[12] S. Du, Y. Shi, D. Zhang et al., "High-peak powermulti-wavelength picosecond pulses generated from a $BaWO_4$ Raman-seeded optical parametric amplifier," *Optics Communications*, vol. 282, no. 14, pp. 2960–2963, 2009.

[13] P. Černý, P. G. Zverev, H. Jelínková, and T. T. Basiev, "Efficient Raman shifting of picosecond pulses using $BaWO_4$ crystal," *Optics Communications*, vol. 177, no. 1, pp. 397–404, 2000.

[14] J. Šulc, H. Jelínková, T. T. Basiev et al., "Nd:$SrWO_4$ and Nd:$BaWO_4$ Raman lasers," *Optical Materials*, vol. 30, no. 1, pp. 195–197, 2007.

[15] L. Li, X. Zhang, Z. Liu et al., "A high power diode-side-pumped Nd:YAG/$BaWO_4$ Raman laser at 1103 nm," *Laser Physics*, vol. 23, Article ID 045402, 2013.

[16] J. Zhao, X. Zhang, X. Guo, X. Bao, L. Li, and J. Cui, "Diode-pumped actively Q-switched Tm, Ho:GdVO4/$BaWO_4$ intracavity Raman laser at 2533 nm," *Optics Letters*, vol. 38, pp. 1206–1208, 2013.

[17] L. Gao, Q. P. Wang, X. Y. Zhang et al., "High-power Nd:YVO_4/$BaWO_4$ intracavity Raman laser emitting at 1103 nm," *Applied Physics B*, vol. 109, pp. 9–13, 2012.

[18] H. Shi, L. Qi, J. Ma, and H. Cheng, "Synthesis of single crystal $BaWO_4$ nanowires in catanionic reverse micelles," *Chemical Communications*, no. 16, pp. 1704–1705, 2002.

[19] D. Li, H. Wu, Z. Li et al., "Multi-phase equilibrium microemulsions-based routes to synthesize nanoscale $BaWO_4$ spheres, cylinders and rods," *Colloids and Surfaces A*, vol. 274, no. 1–3, pp. 18–23, 2006.

[20] B. Xie, Y. Wu, Y. Jiang et al., "Shape-controlled synthesis of $BaWO_4$ crystals under different surfactants," *Journal of Crystal Growth*, vol. 235, no. 1–4, pp. 283–286, 2002.

[21] H. Shi, L. Qi, J. Ma, and H. Cheng, "Polymer-directed synthesis of penniform $BaWO_4$ nanostructures in reverse micelles," *Journal of the American Chemical Society*, vol. 125, no. 12, pp. 3450–3451, 2003.

[22] J. Liu, Q. Wu, and Y. Ding, "Controlled synthesis of different morphologies of $BaWO_4$ crystals through biomembrane/organic-addition supramolecule templates," *Crystal Growth and Design*, vol. 5, no. 2, pp. 445–449, 2005.

[23] S. Kwan, F. Kim, J. Akana, and P. Yang, "Synthesis and assembly of $BaWO_4$ nanorods," *Chemical Communications*, no. 5, pp. 447–448, 2001.

[24] T. Fujita, S. Yamaoka, and O. Fukunaga, "Pressure induced phase transformation in $BaWO_4$," *Materials Research Bulletin*, vol. 9, no. 2, pp. 141–146, 1974.

[25] S. H. Yoon, D.-W. Kim, S.-Y. Cho, and K. S. Hong, "Investigation of the relations between structure and microwave dielectric properties of divalent metal tungstate compounds," *Journal of the European Ceramic Society*, vol. 26, no. 10-11, pp. 2051–2054, 2006.

[26] P. Parhi, T. N. Karthik, and V. Manivannan, "Synthesis and characterization of metal tungstates by novel solid-state metathetic approach," *Journal of Alloys and Compounds*, vol. 465, no. 1-2, pp. 380–386, 2008.

[27] F. Zhang, S.-P. Yang, H.-M. Chen, Z.-H. Wang, and X.-B. Yu, "The effect of an anionic starburst dendrimer on the crystallization of $BaWO_4$ under hydrothermal reaction conditions," *Journal of Crystal Growth*, vol. 267, no. 3-4, pp. 569–573, 2004.

[28] W.-S. Cho and M. Yoshimura, "Hydrothermal, hydrothermal-electrochemical and electrochemical synthesis of highly crystallized barium tungstate films," *Japanese Journal of Applied Physics*, vol. 36, no. 3, pp. 1216–1222, 1997.

[29] L. Zhang, J.-S. Dai, L. Lian, and Y. Liu, "Dumbbell-like $BaWO_4$ microstructures: surfactant-free hydrothermal synthesis, growth mechanism and photoluminescence property," *Superlattices and Microstructures*, vol. 54, pp. 87–95, 2013.

[30] L. I. Ivleva, I. S. Voronina, P. A. Lykov, L. Y. Berezovskaya, and V. V. Osiko, "Growth of optically homogeneous $BaWO_4$ single crystals for Raman lasers," *Journal of Crystal Growth*, vol. 304, no. 1, pp. 108–113, 2007.

[31] D. Ran, H. Xia, S. Sun, Z. Ling, W. Ge, and H. Zhang, "Thermal conductivity of $BaWO_4$ single crystal," *Materials Science and Engineering B*, vol. 130, no. 1–3, pp. 206–209, 2006.

[32] A. K. Chauhan, "Czochralski growth and radiation hardness of $BaWO_4$ crystals," *Journal of Crystal Growth*, vol. 254, no. 3-4, pp. 418–422, 2003.

[33] W. Ge, H. Zhang, J. Wang et al., "The thermal and optical properties of $BaWO_4$ single crystal," *Journal of Crystal Growth*, vol. 276, no. 1-2, pp. 208–214, 2005.

[34] B. N. Roy and M. R. Roy, "Estimation of activation parameters for diffusion-controlled crystallization of barium tungstate from sodium tungstate melts by differential thermal analysis," *Crystal Research and Technology*, vol. 16, pp. 1267–1271, 1981.

[35] F. M. Pontes, M. A. M. A. Maurera, A. G. Souza et al., "Preparation, structural and optical characterization of $BaWO_4$ and $PbWO_4$ thin films prepared by a chemical route," *Journal of the European Ceramic Society*, vol. 23, no. 16, pp. 3001–3007, 2003.

[36] Y. Shen, W. Li, and T. Li, "Microwave-assisted synthesis of $BaWO_4$ nanoparticles and its photoluminescence properties," *Materials Letters*, vol. 65, no. 19-20, pp. 2956–2958, 2011.

[37] C. S. Lim, "Solid-state metathetic synthesis of BaMO4 (M = W, Mo) assisted by microwave irradiation," *Journal of Ceramic Processing Research*, vol. 12, no. 5, pp. 544–548, 2011.

[38] K. Kim and Y. -D. Huh, "Facile synthesis of $BaWO_4$ sub-micron sized octahedron via a microemulsion method," *Bulletin-Korean Chemical Society*, vol. 33, no. 10, pp. 3489–3492, 2012.

[39] K. C. Patil, "Advanced ceramics: combustion synthesis and properties," *Bulletin of Materials Science*, vol. 16, no. 6, pp. 533–541, 1993.

[40] T. T. Basiev, A. A. Sobol, Y. K. Voronko, and P. G. Zverev, "Spontaneous Raman spectroscopy of tungstate and molybdate crystals for Raman lasers," *Optical Materials*, vol. 15, no. 3, pp. 205–216, 2000.

[41] S. Desgreniers, S. Jandl, and C. Carlone, "Temperature dependence of the Raman active phonons in $CaWO_4$, $SrWO_4$ and $BaWO_4$," *Journal of Physics and Chemistry of Solids*, vol. 45, no. 11-12, pp. 1105–1109, 1984.

[42] M. Anicete-Santos, F. C. Picon, C. N. Alves, P. S. Pizani, J. A. Varela, and E. Longo, "The role of short-range disorder in $BaWO_4$ crystals in the intense green photoluminescence," *Journal of Physical Chemistry C*, vol. 115, no. 24, pp. 12180–12186, 2011.

[43] D. L. Wood and J. Tauc, "Weak absorption tails in amorphous semiconductors," *Physical Review B*, vol. 5, no. 8, pp. 3144–3151, 1972.

[44] M. Tyagi, S. G. Singh, A. K. Chauhan, and S. C. Gadkari, "First principles calculation of optical properties of $BaWO_4$: a study by full potential method," *Physica B*, vol. 405, no. 21, pp. 4530–4535, 2010.

[45] W. F. Zhang, Z. Yin, and M. S. Zhang, "Study of photoluminescence and electronic states in nanophase strontium titanate," *Applied Physics A*, vol. 70, no. 1, pp. 93–96, 2000.

[46] H. W. Eng, P. W. Barnes, B. M. Auer, and P. M. Woodward, "Investigations of the electronic structure of d0 transition metal oxides belonging to the perovskite family," *Journal of Solid State Chemistry*, vol. 175, no. 1, pp. 94–109, 2003.

[47] L. S. Cavalcante, J. C. Sczancoski, R. L. Tranquilin et al., "$BaMoO_4$ powders processed in domestic microwave-hydrothermal: synthesis, characterization and photoluminescence at room temperature," *Journal of Physics and Chemistry of Solids*, vol. 69, no. 11, pp. 2674–2680, 2008.

[48] O. S. Heavens, *Optical Properties of Thin Solid Films*, Dover, New York, NY, USA, 1965.

[49] E. Marquez, J. Ramirez-Malo, P. Villares, R. Jimenez-Garay, P. J. S. Ewen, and A. E. Owen, "Calculation of the thickness and optical constants of amorphous arsenic sulphide films from their transmission spectra," *Journal of Physics D*, vol. 25, no. 3, pp. 535–541, 1992.

[50] D. Wahl, V. B. Mikhailik, and H. Kraus, "The Monte-Carlo refractive index matching technique for determining the input parameters for simulation of the light collection in scintillating crystals," *Nuclear Instruments and Methods in Physics Research A*, vol. 570, no. 3, pp. 529–535, 2007.

[51] E. Márquez, A. M. Bernal-Oliva, J. M. González-Leal et al., "Optical-constant calculation of non-uniform thickness thin films of the Ge10As15Se75 chalcogenide glassy alloy in the sub-band-gap region (0.1-1.8 eV)," *Materials Chemistry and Physics*, vol. 60, no. 3, pp. 231–239, 1999.

[52] F. Tepehan and N. Özer, "A simple method for the determination of the optical constants, n and k of cadmium sulfide films from transmittance measurements," *Solar Energy Materials and Solar Cells*, vol. 30, no. 4, pp. 353–365, 1993.

[53] J. H. Ryu, J.-W. Yoon, C. S. Lim, W.-C. Oh, and K. B. Shim, "Microwave-assisted synthesis of CaMoO4 nano-powders by a citrate complex method and its photoluminescence property," *Journal of Alloys and Compounds*, vol. 390, no. 1-2, pp. 245–249, 2005.

[54] E. S. Kim, S. H. Kim, and B. I. Lee, "Low-temperature sintering and microwave dielectric properties of $CaWO_4$ ceramics for LTCC applications," *Journal of the European Ceramic Society*, vol. 26, no. 10-11, pp. 2101–2104, 2006.

[55] H. Zhuang, Z. Yue, F. Zhao, and L. Li, "Low-temperature sintering and microwave dielectric properties of $Ba_5Nb_4O_{15}$-$BaWO_4$ composite ceramics for LTCC applications," *Journal of the American Ceramic Society*, vol. 91, no. 10, pp. 3275–3279, 2008.

[56] H. Zhuang, Z. Yue, F. Zhao, J. Pei, and L. Li, "Microstructure and microwave dielectric properties of $Ba_5Nb_4O_{15}$-$BaWO_4$ composite ceramics," *Journal of Alloys and Compounds*, vol. 472, no. 1-2, pp. 411–415, 2009.

[57] H. Zhuang, Z. Yue, S. Meng, F. Zhao, and L. Li, "Low-temperature sintering and microwave dielectric properties of $Ba_3(VO_4)_2$-$BaWO_4$ ceramic composites," *Journal of the American Ceramic Society*, vol. 91, no. 11, pp. 3738–3741, 2008.

[58] N. K. James, S. Rajesh, K. P. Murali, K. Stanly Jacob, and R. Ratheesh, "Preparation and microwave characterization of $BaWO_4$ filled polytetrafluoroethylene laminates for microwave substrate applications," *Journal of Materials Science*, vol. 21, no. 12, pp. 1255–1261, 2010.